[CANCER RESEARCH 64, 4069–4077, June 15, 2004]

Advances in Brief

Adenovirus-Mediated Expression of Antisense Urokinase Plasminogen Activator Receptor and Antisense Cathepsin B Inhibits Tumor Growth, Invasion, and Angiogenesis in Gliomas

Christopher S. Gondi,[1] Sajani S. Lakka,[1] Niranjan Yanamandra,[1] William C. Olivero,[2] Dzung H. Dinh,[2] Meena Gujrati,[3] C. H. Tung,[4] Ralph Weissleder,[4] and Jasti S. Rao[1,2]

[1]Program of Cancer Biology and Department of Biomedical and Therapeutic Sciences, [2]Department of Neurosurgery, and [3]Department of Pathology, University of Illinois College of Medicine, Peoria, Illinois, and [4]Center for Molecular Imaging Research, Massachusetts General Hospital, Harvard Medical School, Charlestown, Massachusetts

Abstract

We have shown previously that urokinase plasminogen activator receptor (uPAR) and cathepsin B are overexpressed during glioma progression, particularly at the leading edge of the tumor. In the present study, we simultaneously down-regulated uPAR and cathepsin B in SNB19 glioma cell monolayer or SNB19 spheroids using an adenoviral vector carrying antisense uPAR and antisense cathepsin B and a combination of these genes as determined by Western blot analysis. The Ad-uPAR-Cath B-infected cells revealed a marked reduction in tumor growth and invasiveness as compared with the parental and vector controls. *In vitro* and *in vivo* angiogenic assays demonstrated inhibition of capillary-like structure formation and microvessel formation after Ad-uPAR-Cath B infection of SNB19 cells when compared with Ad-cytomegalovirus (CMV)-infected or mock-infected controls. Furthermore, using a near infrared fluorescence probe, *in vivo* imaging for cathepsin B indicated low/undetectable levels of fluorescence after injection of the Ad-uPAR-Cath B construct into preestablished s.c. tumors as compared with Ad-CMV-treated and untreated tumors. The effect with bicistronic construct (Ad-uPAR-Cath B) was much higher than with single (Ad-uPAR/Ad-Cath B) constructs. These results indicate that the down-regulation of cathepsin B and uPAR plays a significant role in inhibiting tumor growth, invasion, and angiogenesis. Hence, the targeting of these two proteases may be a potential therapy for brain tumors and other cancers.

Introduction

The coordinated interaction of different proteolytic systems [*e.g.*, serine proteases, cysteine proteases, and matrix metalloproteases (MMPs)] is essential for tumor cell invasion. The binding of the serine protease urokinase plasminogen activator (uPA) to its receptor (uPAR) is capable of initiating an extracellular cascade of proteolysis that involves the activation of plasminogen and other proteases (1, 2). In addition, these proteolytic cascades release various growth and differentiation factors that are sequestered on the cell surface or within the extracellular matrix (ECM). These factors in turn contribute to the evolution of a migratory or invasive cell phenotype (3). uPAR is a glycosylphosphatidylinositol-linked membrane protein lacking transmembrane and cytosolic domains that participates in the localization of plasminogen activation at the cell surface (4). This cell surface activity facilitates cellular movement via ECM degradation, which is necessary for tumor cell invasion, chemotaxis, and cellular adhesion (5, 6). Our findings and those of others have suggested that the levels of uPA and its receptor present in glioblastomas are much higher than those found in low-grade gliomas (7, 8). Previous studies have shown that the uPAR antibody reduces tumor cell invasion in glioblastomas and colon cancer (9, 10). Similarly, reducing uPAR levels using antisense oligonucleotides also was found to inhibit tumor growth, invasion, and metastasis in some cancers (11, 12). We have designed previously an antisense vector against uPAR that depleted uPAR mRNA and receptors, which in turn inhibited glioma cell invasion *in vitro* as assessed by Matrigel and spheroid models and hindered tumor formation *in vivo* (13, 14). However, because of the nature of the proteolytic cascade, which is believed to facilitate ECM and basement degradation, control of uPAR alone may not be sufficient for complete inhibition of tumor growth and invasion.

Researchers traditionally presumed that only proteases outside the tumor cell were important for tumor cell invasion, but recent data suggest that intracellular proteolysis also is significant (15). The cysteine protease cathepsin B is a lysosomal acid hydrolase with a broad range of endopeptidase activity against substrates and has been found in association with the plasma membrane fraction of tumor cells and in the tumor cell media (16). Up-regulation, membrane association, and secretion of cathepsin B have been shown to occur in many tumor types, including gastric, lung, colon, breast, brain, and prostate (16–21). Cathepsin B also has been shown to initiate the pro-uPA/uPAR/plasminogen/plasmin proteolytic cascade, which ultimately activates latent transforming growth factor β (22). In addition to the indirect activation of MMPs via the uPA/uPAR/plasminogen/plasmin cascade mentioned previously, cathepsin B also may directly activate MMPs (*e.g.*, interstitial collagenase and stromelysin-1; Ref. 23). It was reported previously that membrane-associated cathepsin B might be important for the conversion of pro-uPA to high molecular weight-uPA (24) and uPA, on binding uPAR, and is able to increase the expression of its receptor on the cell surface of uPAR-transfected kidney cells through a post-transcriptional mechanism (25). Given these findings, cathepsin B may well be an important upstream regulator in the activation of pro-uPA/plasminogen and pro-MMPs. We and others have demonstrated that cathepsin B levels significantly increase during glioma progression and are strongly correlated with clinical evidence of invasion (20, 26–29). Furthermore, recent studies have shown that antisense cathepsin B and sense cystatin C, an inhibitor of cathepsin B, stable clones are less invasive in *in vitro* models and formed small tumors in nude mice (30, 31).

In view of the high uPAR and cathepsin B levels in gliomas and other cancers, we hypothesized that the targeting of two different tumor-relevant proteolytic systems with a single treatment could have a significant therapeutic potential. We subsequently constructed a replication-deficient adenovirus expressing antisense transcripts for uPAR and cathepsin B (Ad-uPAR-Cath B). The present study demonstrates that the inhibition of uPAR and cathepsin B did have more

Received 4/7/04; accepted 4/13/04.

Grant support: National Cancer Institute Grant CA 75557, CA 76350, CA 85216, and CA 92393 (J. S. Rao).

The costs of publication of this article were defrayed in part by the payment of page charges. This article must therefore be hereby marked *advertisement* in accordance with 18 U.S.C. Section 1734 solely to indicate this fact.

Requests for reprints: Jasti S. Rao, University of Illinois College of Medicine at Peoria, Program of Cancer Biology, Box 1649, Peoria, IL 61656. Phone: 309-671-3445; Fax: 309-671-3442.

of an effect in suppressing glioma growth, migration, invasion, and angiogenesis. These results suggest that the targeting of multiple proteases is a potentially useful gene therapy approach for the management of human brain tumors and other cancers.

Materials and Methods

Construction of Ad-uPAR-Cath B. We have reported previously the construction of a shuttle vector capable of expressing an antisense transcript at the 5′ region of the human *uPAR* gene with a CMV promoter and BGH polyadenylation signal (pAd-uPAR; Ref. 32). For the present study, we subcloned a 1.150-kb fragment of the 5′ end of the cathepsin B cDNA in an antisense orientation driven by its own independent CMV promoter and BGH polyadenylation terminator into the pAd-uPAR construct. The sequence of the resulting clone pAd-uPAR-Cath B was confirmed. The plasmid construct then was cotransfected with a pJM17 vector in human embryonic kidney 293 cells for isolation of the recombinant adenovirus. The production and screening of adenoviral recombinants and the infection conditions of cells in culture have been described previously (Fig. 1; Ref. 32). Adenovirus single construct for antisense cathepsin B also was constructed using the same 1.150-kb antisense with CMV promoter and BGH polyadenylation signal terminator. The control virus (Ad-CMV) was constructed with a CMV promoter and BGH polyadenylation signal but no gene insert in the E1-deleted region.

Cell Culture and Infection Conditions. SNB19 (human glioblastoma) cells were cultured in DMEM/F-12 supplemented with 10% FCS, L-glutamine (200 μg/ml), 100 units/ml penicillin, and 100 μg/ml streptomycin. Cells were maintained in a humidified atmosphere containing 5% CO_2 at 37°C. The human embryonic kidney cell line 293 was obtained from the American Type Culture Collection (Manassas, VA) and was grown in the same medium as used for glioma cell lines. Viral stocks were suitably diluted in serum-free medium to obtain the desired multiplicity of infection (MOI) or plaque-forming unit and added to cell monolayers and tumor cell spheroids (1 ml/60-mm dish or 3 ml/100-mm dish), and the cells then were incubated at 37°C for 30 min. The necessary amount of culture medium with 10% FCS was added, and cells were incubated for the desired time periods.

Western Blot Analysis. At the end of different incubation periods, control and infected (Ad-CMV, Ad-uPAR, Ad-Cath B, or Ad-uPAR-Cath B) glioma cells and glioma spheroids with various doses of constructs were lysed with an NP-40 buffer containing 0.3% NP-40, 142 mM KCl, 5 mM $MgCl_2$, 2 mM EDTA, 20 mM HEPES (pH 7.4), and a mixture of protease inhibitors (aprotinin, leupeptine, and phenylmethylsulfonyl fluoride; Sigma, St. Louis, MO). Total protein (10–50 μg) was separated on a 12% SDS-PAGE gel and subsequently transferred to a polyvinylidene difluoride membrane (Bio-Rad, Hercules, CA). The membranes were blocked with 6% nonfat dry milk and probed with rabbit antihuman uPAR antibody (R&D Systems, Minneapolis, MN) or antihuman cathepsin B antibody (Athens Research and Technology Inc., Athens, GA). Appropriate antibody conjugated with horseradish peroxidase was used as the secondary antibody, and membranes were developed according to an enhanced chemiluminescence protocol as per manufacturer's instructions (Amersham Biosciences, Piscataway, NJ).

Cell Migration from Spheroids. SNB19 cells (2×10^5/ml) were grown as multicellular tumor spheroids on 100-mm tissue culture plates coated with 0.75% agar. Six to eight spheroids measuring ~150 μm in diameter (~4×10^4 cells/spheroid) were selected for each group and transfected with either Ad-CMV or Ad-uPAR-Cath B at the indicated MOIs. Seventy-two h later, a single glioma spheroid was placed in the center of each vitronectin-coated (50 μg/ml) well of 96-well microplates, and 200 μl of serum-free medium were added to each well. Spheroids were cultured at 37°C for 48 h, after which the spheroids

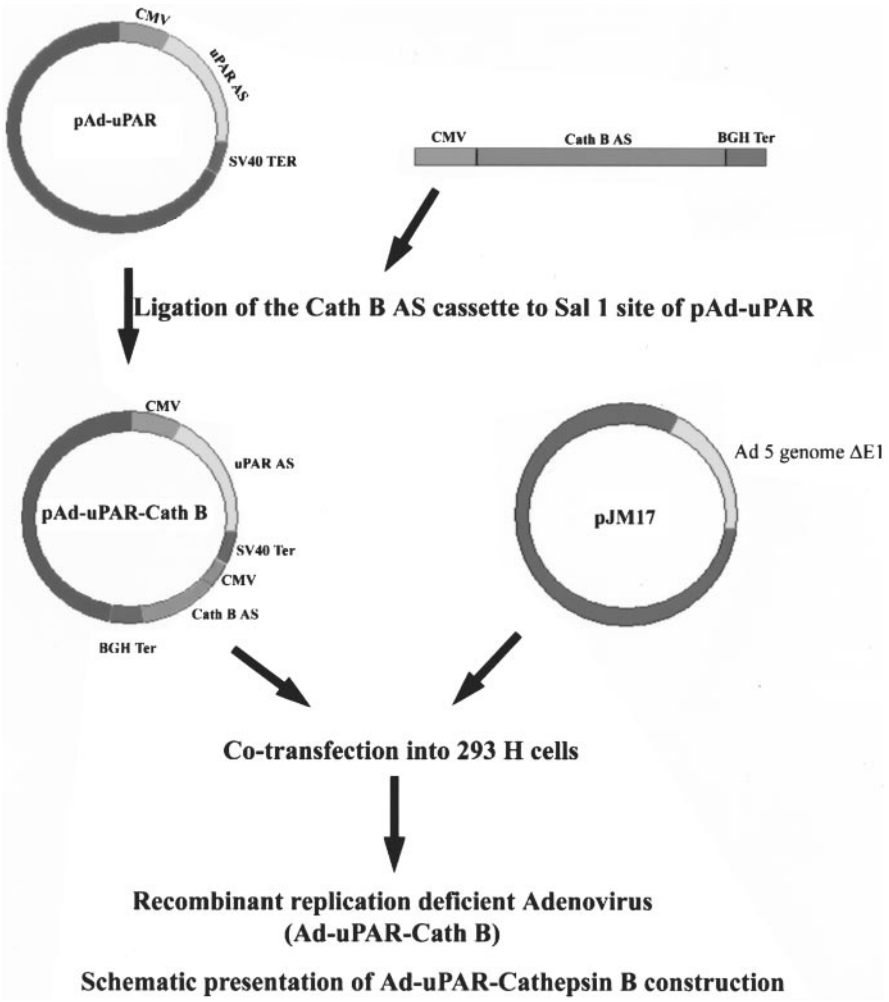

Fig. 1. Schematic presentation of Ad-uPAR-cathepsin B bicistronic construction. Antisense urokinase plasminogen activator receptor (*uPAR*) previously was cloned into polyadenylation signal (*pAd*) vector to generate pAd-uPAR plasmid, which was used as the backbone for the construction of pAd-uPAR-Cath B. Cathepsin B was cloned into the pcDNA 3 vector in the antisense orientation, and the expression cassette containing cytomegalovirus (*CMV*) promoter, antisense cathepsin B, and BGH poly(A) terminator was PCR amplified using the high-fidelity pfx polymerase (Invitrogen, Carlsbad, CA) to incorporate *Sal*I sites in the 5′ and 3′ ends of the expression cassette. This antisense expression cassette was cloned into the *Sal*I sites of pAd-uPAR to generate the bicistronic plasmid pAd-uPAR-Cath B. pAd-uPAR-Cath B then was cotransfected with pJM17 plasmid containing the adenovirus 5 genome with deleted E1 region into 293H cells to generate replication-deficient Ad-uPAR-Cath B adenovirus.

were fixed and stained with Hema-3 (Ficher Diagnostics, Middletown, VA) and photographed. The migration of cells from the center of the spheroids to monolayers was measured using a microscope calibrated with a stage and ocular micrometer and used as an index of cell migration.

Matrigel Invasion Assay. The invasion assay was performed as described previously (13). Briefly, SNB19 cells were infected with 100 MOI of Ad-CMV, Ad-uPAR, Ad-Cath B, or Ad-uPAR-Cath B for 4 days, trypsinized, and counted. A total of 1×10^6/500 μl cells of each treatment condition were added in triplicate to Matrigel-coated porous upper chamber inserts (Collaborative Research, Inc., Boston, MA) and placed in transwell chamber plates (Costar, Corning, NY). The cells then were allowed to invade for 24 h and quantitated as described previously and expressed as a percentage of the sum of cells in the upper and lower wells (13). Cells on the lower side of the membrane were fixed, stained with Hema-3, and photographed.

Spheroid Invasion Assay. SNB19 cells (3×10^5/ml) and fetal rat brain cells (2×10^6/ml) were cultured in low-attachment 35-mm Petri dishes with constant shaking at 60 rpm until multicellular spheroids were formed. Selected spheroids consisted of $\sim 1 \times 10^4$ cells with a diameter of 100–200 μm and were infected with the indicated MOI of either Ad-CMV or Ad-uPAR-Cath B. Seventy-two h later, tumor spheroids were stained with the fluorescent dye DiI and confronted with fetal rat brain aggregates stained with DiO. Progressive destruction of fetal rat brain aggregates and invasion of SNB19 cells were observed with confocal laser scanning microscopy and photographed as described previously (14). The remaining volume of brain aggregates or tumor spheroid during the cocultures in the presence of these constructs was determined as described previously (14).

***In Vitro* Angiogenic Assay.** SNB19 (2×10^4) cells were grown as monolayers in eight-well chamber slides and infected with the indicated MOI of Ad-CMV, Ad-uPAR, Ad-Cath B, or Ad-uPAR-Cath B. After a 24-h incubation period, the medium was removed and cocultured with 4×10^4 human dermal endothelial cells (Center for Disease Control and Prevention, Atlanta, GA) and incubated for another 72 h. Cells then were fixed in 3.7% formaldehyde and blocked with 2% bovine serum album. Endothelial cells were probed for factor VIII antigen using specific antibody (DAKO Corporation, Carpinteria, CA) for 1 h, following which the cells were washed with PBS and incubated with appropriate FITC-conjugated secondary antibody for 1 h. Finally, the cells were washed and examined with fluorescence microscopy (33). Endothelial cells (4×10^4) alone also were grown in the presence of conditioned media from control, Ad-CMV, Ad-uPAR, Ad-Cath B, or Ad-uPAR-Cath B at the indicated MOI. After 72 h, these cells were fixed in 3.7% formaldehyde and stained with H&E. Image-Pro software (Media Cybernetics, Inc., Silver Spring, MD) was used for quantification of angiogenesis of the FITC-stained cocultures and the H&E-stained cells. The degree of angiogenesis was measured by the following method: number of branch points and the total number of branches per point were counted, with the product indicating the degree of angiogenesis.

***In Vivo* NIRF Imaging.** The design and synthesis of the enzyme-activated near infrared fluorescence (NIRF) probes are described in detail previously (34). Briefly, the probe was a modification of a synthetic graft copolymer consisting of poly-L-lysine that is sterically protected by multiple monomethoxy-polyethylene glycol side chains (35). U87-MG cells (5×10^6) were s.c. injected into nude mice. Eight to 10 days later, when tumor size had reached 4–5 mm, the mice were injected with 5×10^8 plaque-forming units of either Ad-CMV or Ad-uPAR-Cath B every other day for a total of five times.

For s.c. tumors, we used the U87 glioblastoma cell line rather than SNB19 cells because SNB19 cells do not form solid tumors s.c. but rather tend to migrate and disperse, whereas U87 cells form big, solid tumors. Baseline images in the animals were obtained immediately before injection of the NIRF probe to allow for the evaluation of the spatial distribution of native fluorochrome (*e.g.*, NIRF in the gut). Animals then were injected via the tail vein with 10 nmol of poly-l-lysine/methoxypolyethylene glycol graft copolymer (PGC) in 100 μl of normal saline. Images were obtained at 72 h using the Kodak image station 440CF (Rochester, NY). Significance of the differences between the NIRF signal mean values of tissues was determined using two-tailed *t* tests and SEM.

Dorsal Skinfold Chamber Model. Athymic nude mice (*nu/nu*; 18 male/female; weight, 28–32 g) were bred and maintained within a specific-pathogen, germ-free environment. The implantation technique of the dorsal skinfold chamber model has been described previously (36) Sterile small-animal surgical techniques were followed. Mice were anesthetized by i.p. injection with ketamine (50 mg/kg) and xylazine (10 mg/kg). Once the animal was anesthetized completely, a dorsal air sac was made in the mouse by injecting 10 ml of air. Diffusion chambers (Fisher Scientific, Hampton, NH) were prepared by aligning a 0.45-μm Millipore membrane (Fisher Scientific) on both sides of the rim of the "O" ring (Fisher Scientific) with sealant. Once the chambers were dry (2–3 min), they were sterilized by UV radiation for 20 min. Twenty μl of PBS were used to wet the membranes. A total of 2×10^6 SNB19 cells infected with mock or Ad-CMV (100 MOI) or Ad-uPAR-Cath B (50 MOI) were suspended in 100–150 μl of sterile PBS and injected into the chamber through the opening of the "O" ring. The opening was sealed by a small amount of bone wax. A 1.5–2-cm superficial incision is made horizontally along the edge of the dorsal air sac, and the air sac is opened. With the help of forceps, the chamber was placed underneath the skin and sutured carefully. After 10 days, the animals were anesthetized with ketamine and xylazine and sacrificed by intracardiac perfusion with saline (10 ml), followed by 10 ml of 10% formalin/0.1 M phosphate solution, followed by 0.001% FITC solution in PBS. The animals were carefully skinned around the implanted chambers, and the implanted chambers were removed from the s.c. air fascia. The skinfold covering the chambers was photographed under visible light and for FITC fluorescence. The number of blood vessels within the chamber in the area of the air sac fascia was counted, and their lengths were measured.

Animal Experiments. SNB19 cells that stably express green fluorescent protein (GFP) were infected in culture with either 100 MOI of Ad-CMV, Ad-uPAR, and Ad-Cath B or 50 MOI and 100 MOI of Ad-uPAR-Cath B for 5 days, trypsinized, counted, and injected intracranially into nude mice. After a 5-week follow-up period (*e.g.*, when the control mice start showing symptoms), the mice were sacrificed via cardiac perfusion with formaldehyde as described previously (14). The brains were removed and fixed in 10% formaldehyde in PBS for 12 h. Following fixation, the brains were embedded in paraffin and sectioned as per standard protocols (14). Sections were stained with H&E to reveal tumor growth. The sections were blindly reviewed and scored for the size of the tumor in each case semiquantitatively. The average cross-sectional diameter measured in sections of each tumor was used to measure tumor size and compared between controls and antisense transfectants. The variation between the sections in each group was $<10\%$. Fluorescence microscopy was performed on tumor sections for GFP-expressing cells on plain deparaffinized, rehydrated sections and quantitated using Image-Pro Discovery software (Media Cybernetics, Silver Spring, MD).

Results

Ad-uPAR-Cath B Infection Decreased uPAR and Cathepsin B Protein Levels. We inserted two genes in an antisense orientation for a serine protease receptor (uPAR) and a lysosomal protein (cathepsin B) with their own independent CMV promoters into an E1-deleted recombinant adenovirus. To characterize the properties of the transcripts expressed from the engineered adenovirus, we infected proliferating SNB19 glioma tumor cells at the indicated MOIs of Ad-CMV, Ad-uPAR, Ad-Cath B, and Ad-uPAR-Cath B. Five days later, we harvested the cells and immunoblotted the lysate for uPAR and cathepsin B. Fig. 2*A* shows that the uPAR protein band (M_r 60,000) was decreased in a dose-dependent fashion. With the Ad-uPAR-Cath B construct, uPAR protein levels decreased 50% at 10 MOI and 90% at 50 MOI as compared with the Ad-CMV-infected and mock-infected constructs. Fig. 2*B* shows that the decrease in uPAR protein also was related to time. In particular, the SNB19 cells infected with the bicistronic construct at 50 MOI showed a significant decrease by day 3, and by day 4 the decrease had reached 90%. Ad-uPAR also decreased the levels of uPAR at 100 MOI and fivefold to sixfold less compared with Ad-uPAR-Cath B at the same MOI (Fig. 2, *A* and *B*). There similarly were significant decreases in cathepsin B protein levels in the cells infected with Ad-Cath B (100 MOI) and Ad-uPAR-Cath B at 10 MOI and 50 MOI as compared with the mock-, Ad-CMV-, and Ad-uPAR-infected cells (Fig. 2*C*). The reduction in cathepsin B levels also was related to time; SNB19 cells infected with 50 MOI of Ad-uPAR-Cath B showed a 90% decrease in cathepsin B

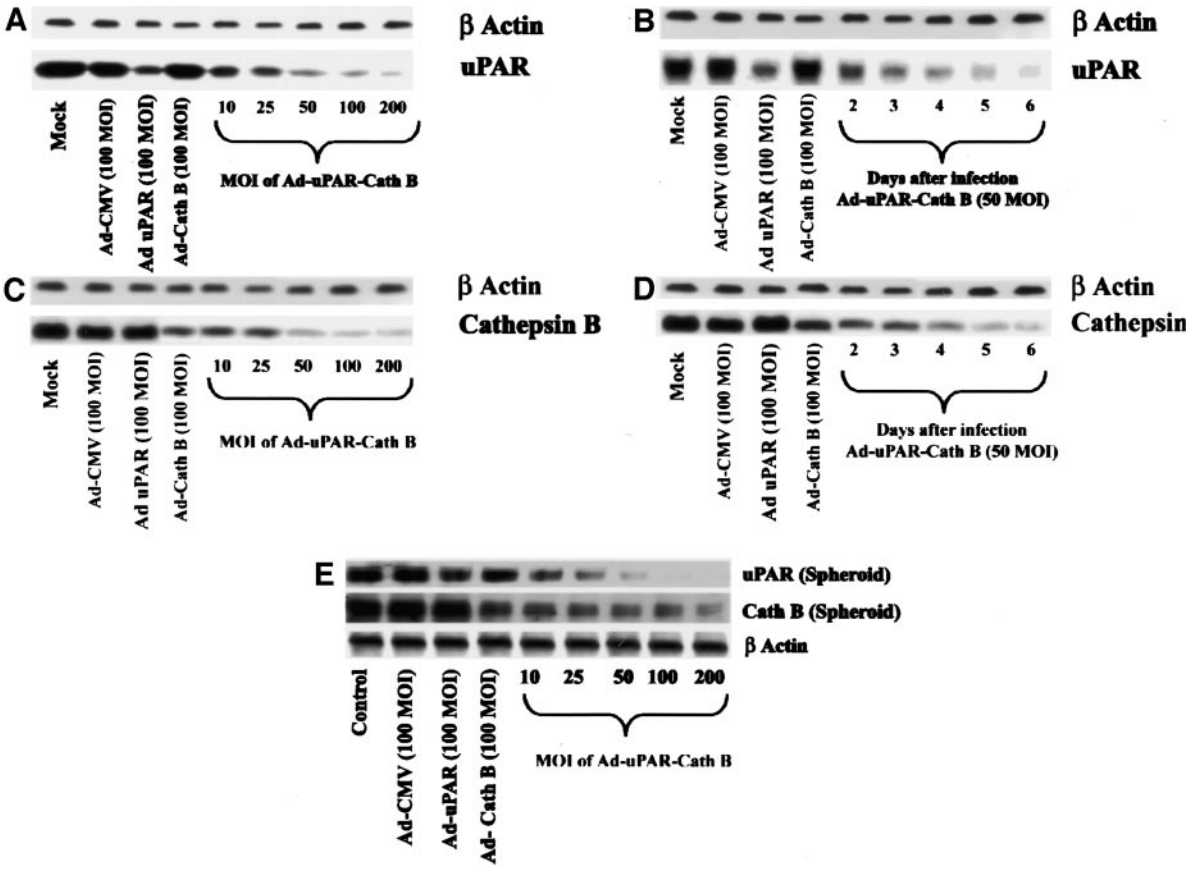

Fig. 2. Immunoblot analysis of urokinase plasminogen activator receptor (*uPAR*) and cathepsin B. SNB19 cells were transfected with Ad-cytomegalovirus (*CMV*), Ad-uPAR, Ad-Cath B, or Ad-uPAR-Cath B at the indicated multiplicity of infection (*MOI*). After 5 days of incubation, cell lysates were prepared in extraction buffer, and uPAR (*A*) and cathepsin B (*C*) levels were determined by Western blot analysis. SNB19 cells were infected with 50 MOI at different time intervals, and the expression of uPAR (*B*) and cathepsin B (*D*) protein levels were determined by Western blot analysis. SNB19 spheroids were transfected with Ad-CMV, Ad-uPAR, Ad-Cath B, or Ad-uPAR-Cath B at the indicated MOIs (*E*). After 4-day incubation, cell extracts were prepared in extraction buffer, and the levels of uPAR and cathepsin B were determined by Western blot analysis using their specific antibodies (*E*). β-Actin simultaneously was immunodetected to verify the loading of similar amounts of cell lysates.

levels by day 5 when compared with the cells infected with mock, Ad-CMV, and Ad-uPAR constructs (Fig. 2*D*). Ad-Cath B similarly decreased the levels of cathepsin B at 100 MOI, but Ad-uPAR-Cath B significantly decreased sixfold to sevenfold more compared with the single constructs (Fig. 2, *C* and *D*). β-Actin levels did not change under any of these conditions, indicating that similar amounts of protein were loaded. We also determined the effect of these constructs on SNB19 spheroids. Fig. 2*E* shows that Ad-uPAR-Cath B constructs decreased the levels of uPAR and cathepsin B in a dose-dependent manner. The single constructs also reduced the levels of uPAR and cathepsin B, and the effect was lower when compared with bicistronic constructs. These single constructs also were specific to their target molecules.

Ad-uPAR-Cath B Infection Decreased Angiogenesis. To assess whether Ad-uPAR-Cath B can influence tumor-induced angiogenesis in an *in vitro* system, we cocultured human endothelial cells with SNB19 cells. Endothelial cells formed capillary-like structures when cocultured with the SNB19 cells within 24–48 h; however, when plated alone, endothelial cells did not form capillary-like structures. Fig. 3, *A–C*, shows that Ad-uPAR (100 MOI) and Ad-Cath B (100 MOI) repressed capillary formation by ~65% and 45%, respectively, when compared with the mock or Ad-CMV-infected cocultures. In addition, SNB19 cells infected with 25 MOI of Ad-uPAR-Cath B inhibited endothelial capillary formation by ~75%. Moreover, increasing the MOI of the bicistronic construct progressively inhibited capillary-like structure formation in a dose-dependent manner. As indicated in Fig. 3, *A–C*, the effect of the Ad-uPAR-Cath B construct in inhibiting capillary-like structure formation was much higher than Ad-uPAR and Ad-Cath B constructs.

To further demonstrate the effect of Ad-uPAR-Cath B in tumor angiogenesis, we used an experimental *in vivo* model system, the dorsal skinfold chamber assay. Implantation of a chamber containing SNB19 cells resulted in the development of microvessels (as indicated with arrows) with curved thin structures and the absence of FITC fluorescence. SNB19 cells infected with 50 MOI of Ad-uPAR-Cath B did not develop any new vessels, indicating that Ad-uPAR-Cath B infection can inhibit tumor-induced angiogenesis *in vivo* (Fig. 3, *D* and *E*).

Ad-uPAR-Cath B Infection Decreased Migration of Glioma Cells from Spheroids. To determine whether Ad-uPAR-Cath B-mediated inhibition of uPAR and cathepsin B can influence migration, we infected glioma spheroids with various concentrations of the bicistronic vector and observed the migration of cells on vitronectin-coated plates. As seen in Fig. 4*A*, cell migration from Ad-CMV-infected spheroids was significant. In contrast, the migration rate was drastically reduced in spheroids infected with 10 MOI, 25 MOI, and 50 MOI of Ad-uPAR-Cath B in a dose-dependent manner. The migrating capacity of the control/Ad-CMV-infected spheroids was significantly higher ($P < 0.001$) than that of the Ad-uPAR-Cath B-infected spheroids as shown by the number of cells migrated out from the spheroids (Fig. 4*B*).

Ad-uPAR-Cath B Infection Decreased Invasiveness of SNB19 Cells. To study the effect of the Ad-uPAR-Cath B bicistronic vector on glioma invasion, we used two different models (Matrigel and

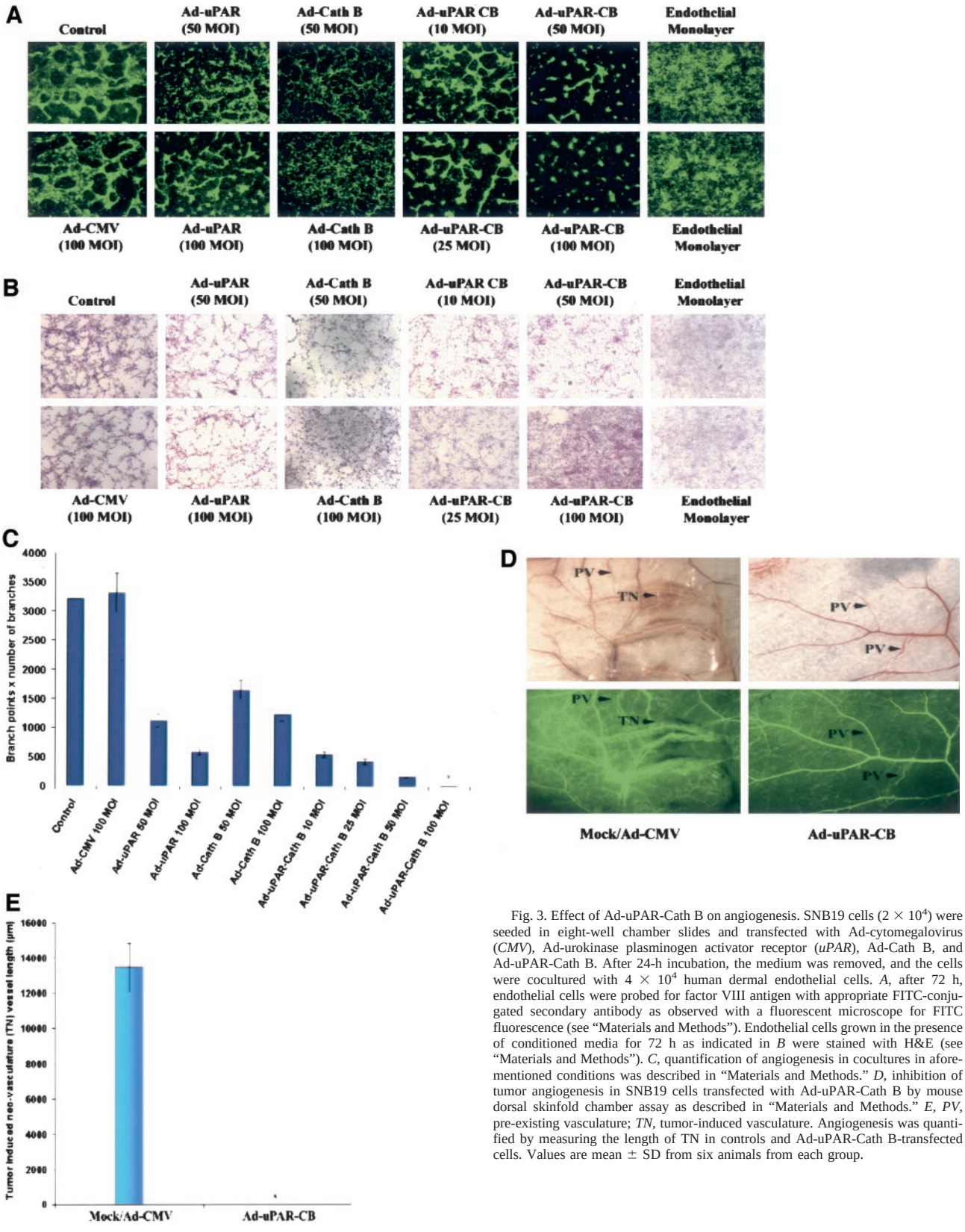

Fig. 3. Effect of Ad-uPAR-Cath B on angiogenesis. SNB19 cells (2×10^4) were seeded in eight-well chamber slides and transfected with Ad-cytomegalovirus (*CMV*), Ad-urokinase plasminogen activator receptor (*uPAR*), Ad-Cath B, and Ad-uPAR-Cath B. After 24-h incubation, the medium was removed, and the cells were cocultured with 4×10^4 human dermal endothelial cells. *A*, after 72 h, endothelial cells were probed for factor VIII antigen with appropriate FITC-conjugated secondary antibody as observed with a fluorescent microscope for FITC fluorescence (see "Materials and Methods"). Endothelial cells grown in the presence of conditioned media for 72 h as indicated in *B* were stained with H&E (see "Materials and Methods"). *C*, quantification of angiogenesis in cocultures in aforementioned conditions was described in "Materials and Methods." *D*, inhibition of tumor angiogenesis in SNB19 cells transfected with Ad-uPAR-Cath B by mouse dorsal skinfold chamber assay as described in "Materials and Methods." *E*, *PV*, pre-existing vasculature; *TN*, tumor-induced vasculature. Angiogenesis was quantified by measuring the length of TN in controls and Ad-uPAR-Cath B-transfected cells. Values are mean ± SD from six animals from each group.

spheroid). Cells infected with Ad-CMV, Ad-uPAR, and Ad-uPAR-Cath B were allowed to invade through Matrigel for 24 h. There was no difference of invading glioma cells infected with Ad-CMV as compared with the mock-infected cells. Only 20–25% of Ad-uPAR-infected cells and 30–35% of Ad-Cath B-infected cells invaded compared with the Ad-CMV-infected cells. In the Ad-uPAR-Cath B-infected cells, a 20-fold (5–7%) decrease in the invasion potential of the glioma cells was seen when compared with the Ad-CMV-infected cells (Fig. 4*C*).

To further investigate the role of Ad-uPAR-Cath B on invasion,

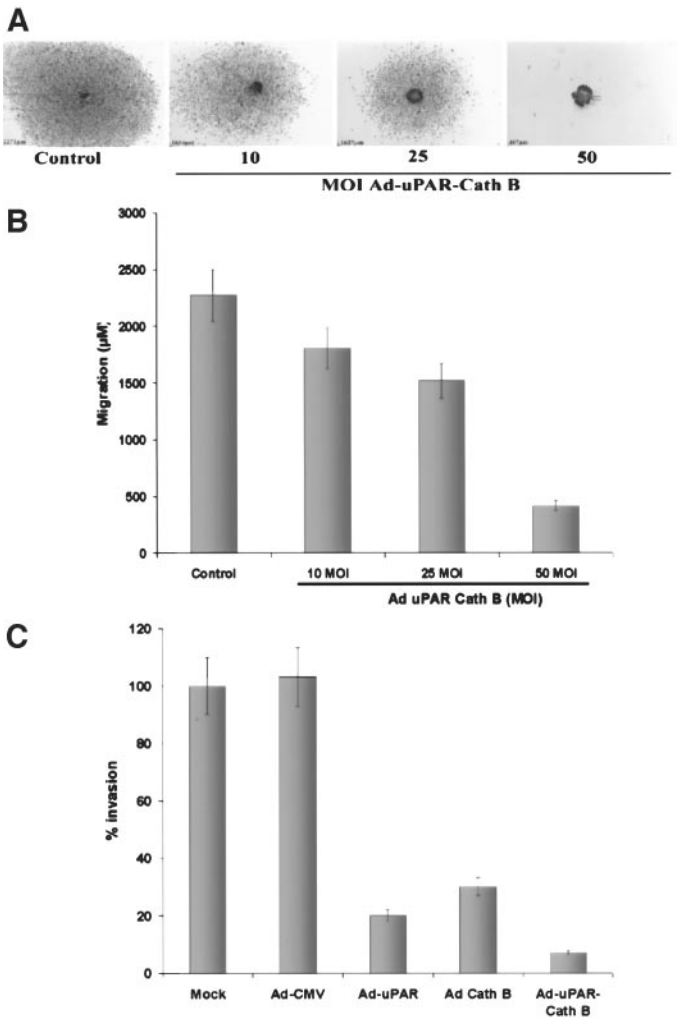

Fig. 4. *A*, effect of Ad-uPAR-Cath B on the migration of SNB19 spheroids. SNB19 spheroids were infected with mock and Ad-uPAR-Cath B, transferred 72 h later to vitronectin-coated (50 μg/ml) 96-well plates, and further incubated for 48 h. The cells then were washed, fixed, and stained with Hema-3. *B*, the migration of cells from the center of the spheroids to the monolayers was measured using a microscope calibrated with a stage and ocular micrometer. The data shown are the mean value ± SD of the results of five independent experiments from each group. Effect of Ad-uPAR-Cath B on glioma invasion. *C*, SNB19 cells were trypsinized 96 h after infection with mock or 100 multiplicity of infection (*MOI*) of Ad-cytomegalovirus (*CMV*), Ad-urokinase plasminogen activator receptor (*uPAR*), Ad-Cath B, and Ad-uPAR-Cath B, washed with PBS, and resuspended in serum-free medium. Invasion assays were carried out in a 12-well transwell unit on a polycarbonate filter with 8-μm pores coated with Matrigel, as described in "Materials and Methods." The percentage of invasion was quantitated as described in "Materials and Methods." Values are mean ± SD from five different experiments.

SNB19 spheroids were infected with Ad-CMV and 10 MOI, 25 MOI, and 50 MOI of Ad-uPAR-Cath B for 5 days and stained with the fluorescent dye DiI (red). These spheroids then were cocultured with fetal rat brain aggregates stained with DiO (green), and images were obtained using confocal microscopy. Ad- CMV-infected spheroids progressively invaded the fetal rat brain aggregates within 72 h. In contrast, Ad-uPAR-Cath B decreased the invasion of glioma spheroids in a dose-dependent manner. A small region of cell colocalization was seen with a spheroid infected with 10 MOI of Ad-uPAR-Cath B, but no invasion of the fetal rat brain aggregates was observed at 72 h. With spheroids infected with 25 MOI of the bicistronic contrast, colocalization was seen but was relatively less than that seen in the 10 MOI-infected spheroids. In spheroids infected with 50 MOI of the virus, glioma spheroids and feta rat brain aggregates remained as two separate entities (Fig. 5*A*). Quantitation of the remaining fetal rat brain aggregates indicated that glioma spheroids infected with Ad-CMV progressively invaded by ~90% at 72 h. However, glioma spheroids infected with Ad-uPAR-Cath B at 10 MOI, 25 MOI, and 50 MOI in cocultures with fetal rat brain aggregates invaded only 15–2% by 72 h (Fig. 5*B*). These data suggest that Ad-uPAR-Cath B suppresses the invasive ability of glioma cells *in vitro*.

Ad-uPAR-Cath B Inhibits Tumor Growth in Mice. To determine whether decreased levels of uPAR and cathepsin B levels could inhibit tumor growth, we infected SNB19 variants that stably express GFP with either Ad-CMV, Ad-uPAR, Ad-Cath B, or Ad-uPAR-Cath B (50 MOI and 100 MOI) for 5 days. The cells were trypsinized, and $2 \times 10^6/10$ μl were injected intracerebrally into nude mice (10 mice in each group). We sacrificed mice after 5 weeks of injections to monitor tumor development. All of the animals in the Ad-CMV-treated group had intact cerebral tumors that were characterized by H&E staining and strong GFP fluorescence (Fig. 5, *C* and *D*). Brain sections of mice injected with 100 MOI of Ad-uPAR or Ad-Cath B had small tumors as illustrated by H&E staining and GFP fluorescence (Fig. 5, *C* and *D*). Brain sections of mice injected with 50 MOI of Ad-uPAR-Cath B had only a small number of residual cells surrounding the injection tract, indicating some tumor growth as illustrated by H&E staining and GFP fluorescence. However, we did not detect any florescence in brain sections from mice injected with cells treated with 100 MOI of the bicistronic construct (Fig. 5, *C* and *D*). Quantification of GFP fluorescence revealed >60% reduction with 100 MOI of Ad-uPAR and >50% reduction with 100 MOI of Ad-Cath B compared with control and Ad-CMV groups (Fig. 5*E*). Quantification of GFP fluorescence also revealed >80% of reduction with 50 MOI of Ad-uPAR-Cath B and no tumor growth with 100 MOI of Ad-uPAR-Cath B compared with control and Ad-CMV groups (Fig. 5*E*).

Inhibition of Cathepsin B Levels in Ad-uPAR-Cath B Tumors as Determined with an NIRF Cathepsin B Probe. NIRF probes have low fluorescence unless activated by the target compound (proteases), can be detected in nanomolar amounts, and have no apparent toxicity at the tested concentrations (37). These probes are highly specific for each protease and can detect the target protease in *in vitro* and *in vivo* models (37–39). *In vivo* imaging of U-87MG tumor-bearing mice demonstrated that the distribution of the NIRF signal was different between the animals infected with Ad-CMV and those infected with Ad-uPAR-Cath B; Ad-CMV-infected animals demonstrated high levels of cathepsin B compared with animals infected with Ad-uPAR-Cath B (Fig. 6). These results clearly demonstrated that established tumor growth was inhibited by treatment with the Ad-uPAR-Cath B construct when compared with the Ad-CMV construct.

Discussion

In addition to vasculature remodeling and destruction of the surrounding normal brain tissue, local invasive infiltration and growth are key features of glioblastoma multiforme. The invasive character of glioblastoma appears to depend partly on the proteolytic destruction of the ECM. Several studies have indicated that proteases are involved in tumor growth and invasion at the primary and metastatic sites (40, 41). The correlation between uPAR (7, 8, 13) and cathepsin B (20, 26–29) expression levels and glioma aggressiveness suggest that cathepsin B and uPAR are important components of the invasive phenotype of gliomas. The use of antisense techniques to silence target genes has been shown to have potential efficacy in cancer therapy. In the present study, we simultaneously targeted these two proteases, uPAR and cathepsin B, using adenovirus-mediated antisense gene delivery. The anticancer effect of Ad-uPAR-Cath B was

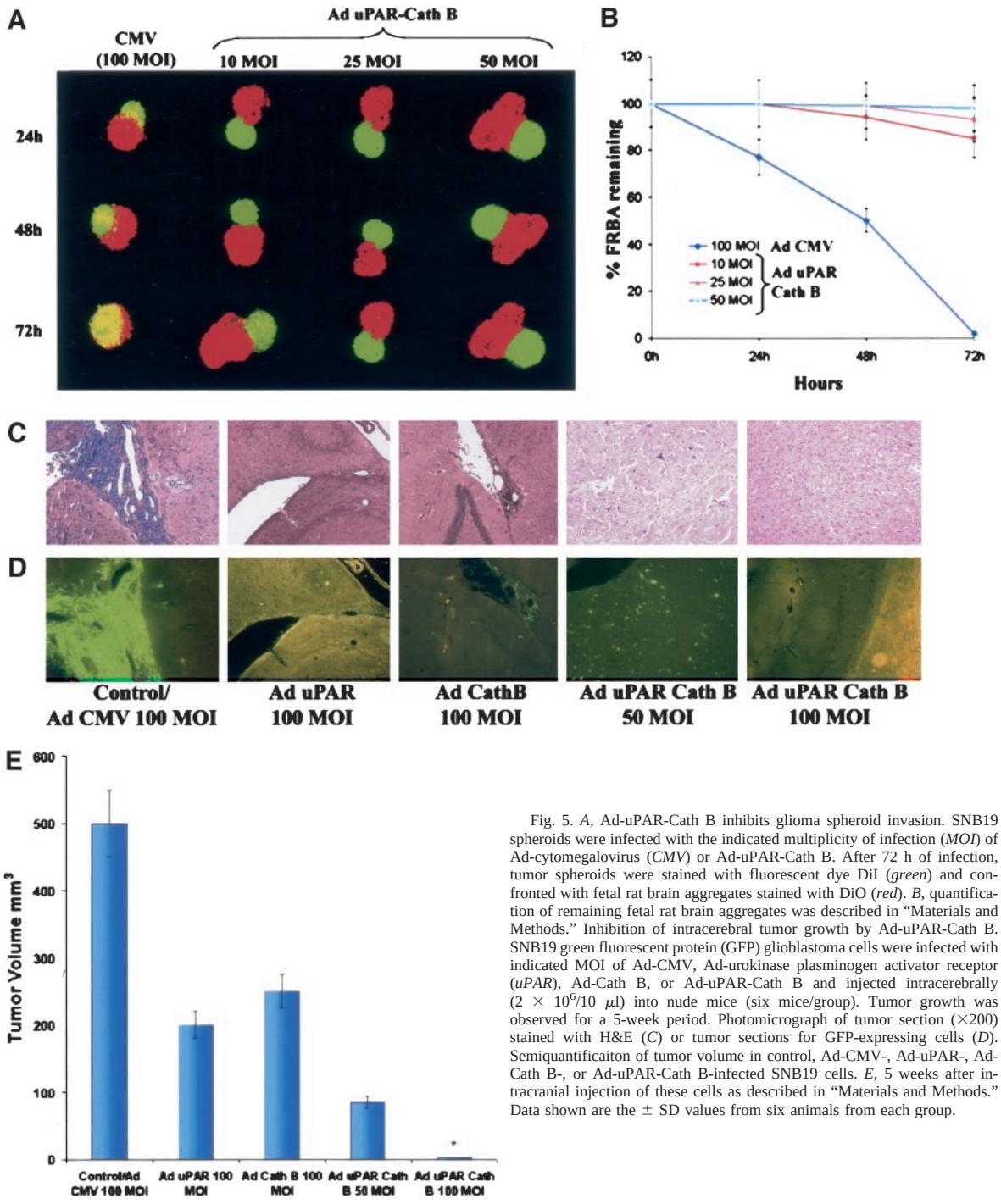

Fig. 5. *A*, Ad-uPAR-Cath B inhibits glioma spheroid invasion. SNB19 spheroids were infected with the indicated multiplicity of infection (*MOI*) of Ad-cytomegalovirus (*CMV*) or Ad-uPAR-Cath B. After 72 h of infection, tumor spheroids were stained with fluorescent dye DiI (*green*) and confronted with fetal rat brain aggregates stained with DiO (*red*). *B*, quantification of remaining fetal rat brain aggregates was described in "Materials and Methods." Inhibition of intracerebral tumor growth by Ad-uPAR-Cath B. SNB19 green fluorescent protein (GFP) glioblastoma cells were infected with indicated MOI of Ad-CMV, Ad-urokinase plasminogen activator receptor (*uPAR*), Ad-Cath B, or Ad-uPAR-Cath B and injected intracerebrally ($2 \times 10^6/10\ \mu l$) into nude mice (six mice/group). Tumor growth was observed for a 5-week period. Photomicrograph of tumor section (×200) stained with H&E (*C*) or tumor sections for GFP-expressing cells (*D*). Semiquantificaiton of tumor volume in control, Ad-CMV-, Ad-uPAR-, Ad-Cath B-, or Ad-uPAR-Cath B-infected SNB19 cells. *E*, 5 weeks after intracranial injection of these cells as described in "Materials and Methods." Data shown are the ± SD values from six animals from each group.

demonstrated with *in vitro* and *in vivo* studies using the SNB19 and U-87MG glioma cell lines. We demonstrated that the simultaneous blockade of uPAR and cathepsin B genes has an additive effect on tumor regression and tumor-induced angiogenesis as compared with our previous study on adenovirus-mediated antisense uPAR in SNB19 cells.

Adenovirus-mediated expression of antisense gene transcripts for uPAR, cathepsin B, and a combination of uPAR and cathepsin B significantly reduced the cellular expression of the uPAR and cathepsin B protein levels in SNB19 monolayers or SNB19 spheroids as determined with their respective antibodies by Western blot analysis. We then determined whether the inhibition of uPAR and cathepsin B could influence the invasive potential of SNB19 cells in two systems: Matrigel and a three-dimensional spheroid model. Ad-uPAR-Cath B infection had a more superior effect in inhibiting glioma invasion compared with Ad-uPAR infection. Our results are in accord with the observations that uPAR and cathepsin B are correlated with the invasive properties of malignant cells. As earlier research indicates, a proteolytic cascade involving multiple proteases facilitates tumor progression, and uPAR levels have been correlated strongly with metastatic potential in human cancer cell lines of the colon, lung, and melanoma (42–45). However, other studies of colon cancer metastasis have shown that antisense uPAR mRNA could only partially control metastasis. The effect of uPAR also could depend on the ratio of uPA

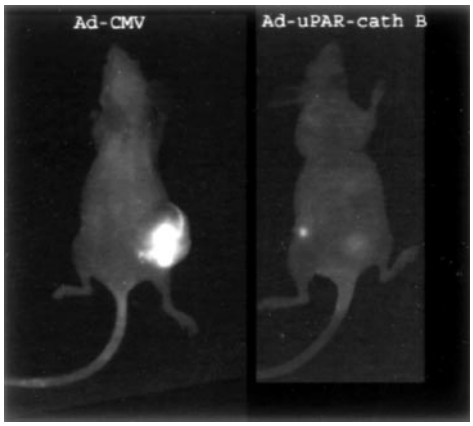

Fig. 6. *In vivo* near infrared fluorescence imaging of s.c. U-87MG tumor growth. U-87MG cells (5×10^6) were s.c. injected into nude mice, and when tumor size reached 4–5 mm, the mice were injected with 5×10^8 plaque-forming units of either Ad-cytomegalovirus (*CMV*) or Ad-uPAR-Cath B every other day for a total of three times. After 4 weeks, animals were injected via the tail vein with 10 nmol of CPGC in 100 μl of normal saline, and images were obtained using Kodak image station 440CF 72 h later.

to uPAR and the levels of their inhibitor plasminogen activator inhibitor 1. Furthermore, other proteases may compensate for the lack of uPA activity and uPAR protein. Cathepsin B is among the candidate proteinases believed to participate in invasion and metastasis. Cathepsin B also can activate the soluble and tumor cell receptor-bound forms of uPA and other latent proteinases (23, 46).

Thus, the effective inhibition of invasion by Ad-uPAR-Cath B could be caused by the additive effect of inhibiting uPAR and cathepsin B.

In addition to the proteolytic degradation of the ECM, tumor progression requires the proliferation of cancer cells via adhesive and migratory events. SNB19 spheroids infected with Ad-uPAR-Cath B demonstrated significantly reduced migration as compared with vector controls at 10 and 25 MOI. Recent studies indicate that uPAR possesses cellular activities, including an ability to generate intracellular signal transduction, regulate integrin function, and directly bind vitronectin (47, 48). Interaction of uPAR and integrins leads to potentiation of integrin-mediated signaling and enhanced cell migration (49). Concomitant with this observation, Ad-uPAR-Cath B-infected SNB19 cells failed to adhere to the vitronectin-coated plates at 50 MOI in the present study. It has been demonstrated that the binding of uPA to its receptor promotes migration and invasion of melanoma cells *in vitro* (45). Adhesion and migration in kidney epithelial and smooth muscle cells were inhibited with the disruption of caveolin-integrin-uPAR complex (50). Increases of cathepsin B mRNA, protein, and/or activity are observed in tumor cells at the invasive edges of many cancers, including infiltrating glioblastomas (20). Using immunofluorescence staining and enzyme histochemistry, it was found that cathepsin B is localized in fibroblasts, leukocytes, and ECM at the invasive front of rabbit V2 carcinoma (51).

In this study, we have demonstrated that the management of intracranial malignant gliomas in nude mice with Ad-uPAR-Cath B was therapeutically effective when compared with the controls and single constructs of Ad-uPAR or Ad-Cath B. SNB19 cells were infected with either empty vector Ad-uPAR, Ad-Cath B, or Ad-uPAR-Cath B (50 MOI and 100 MOI), cultured for 5 days, and then injected into the brains of immunocompromised mice. As the results show, we did not detect any intracranial tumor growth in the mice treated with Ad-uPAR-Cath B compared with Ad-CMV, Ad-uPAR, and Ad-Cath B. Ad-uPAR-Cath B suppresses two different tumor-relevant proteolytic systems, thereby leading to more effective inhibition of tumor growth. *In vivo* imaging of the s.c. tumors with an NIRF probe for cathepsin B also provided evidence of this inhibition; cathepsin B expression was significantly reduced in the bicistronic virus-infected tumors. Imaging techniques like this provide the much-needed clinical verification that protease inhibitors are reaching and reducing the activity of their intended target.

Our results also demonstrate that low concentrations of the bicistronic construct (25 MOI) Ad-uPAR-Cath B was effective in inhibiting capillary-like structure formation in an *in vitro* angiogenic assay in which SNB19 cells were cocultured with human dermal endothelial cells. Tumor progression and the incidence of metastasis are correlated with vascular density (52). Clinical data have shown that malignancy index often is associated with tumor angiogenesis, and angiogenesis inhibition strategies recently have emerged as approaches for cancer management. Immunohistochemical and *in situ* histochemical studies have demonstrated cathepsin B expression in neovessels induced during the malignant progression of human glioblastoma and prostate carcinoma (27, 51). Likewise, strong immunostaining of cathepsin B was observed in rat brain microvascular endothelial cells as they formed capillary tubes *in vitro* (53). Studies have reported that cathepsin B stimulates angiogenesis by inactivating tissue inhibitors of MMPs and thereby indirectly increasing MMP activity, which is angiogenic (54). The importance of the interaction between uPA and uPAR during angiogenesis also has been demonstrated in a number of *in vivo* systems. An octamer peptide derived from the nonreceptor-binding region of uPA was shown to inhibit tumor growth and angiogenesis in breast cancer (55) and in combination with cisplatin in glioblastomas (56). To substantiate *in vitro* results, we also visualized tumor angiogenesis *in vivo* using the dorsal skinfold chamber model for s.c. tumors. This preparation facilitates the real-time analysis of angiogenesis and microcirculation in the tumors. Ad-uPAR-Cath B-infected cells exhibited decreased tumor-induced vasculature when compared with the control cells. We hypothesize that this event could be related to the tumor regression observed in Ad-uPAR-Cath B-treated tumors. Together, these results suggest that uPAR and cathepsin B may contribute synergistically to inhibit glioma invasion and tumor growth by inhibiting angiogenesis.

Increasing evidence suggests that virtually all tumors use proteases to invade the ECM. The level of protease activity may constitute a final common pathway for tumor invasiveness and may be a particularly appropriate target for anti-invasive therapy. Successful limitation of tumor spread by anti-invasive agents at particular stages of tumorigenesis could help to convert an infiltrative tumor into a local tumor, which then could restore efficacy to focal tumor therapies. Because invasiveness constitutes the most destructive characteristic of malignant gliomas and results in poor clinical outcomes, our attempt to simultaneously target uPAR and cathepsin B has clear clinical implications with a potential broad field of action for the management of other cancers, including brain tumors.

Acknowledgments

We thank Karen Minter for preparing the manuscript and Sushma Jasti and Diana Meister for manuscript review.

References

1. Andreasen PA, Egelund R, Petersen HH. The plasminogen activation system in tumor growth, invasion, and metastasis. Cell Mol Life Sci 2000;20;57:25–40.
2. Reuning U, Magdolen V, Wilhelm O, et al. Multifunctional potential of the plasminogen activation system in tumor invasion and metastasis (review). Int J Oncol 1998;13:893–906.
3. Rabbani SA, Mazar AP. The role of the plasminogen activation system in angiogenesis and metastasis. Surg Oncol Clin N Am 2001;10:393–415.
4. Ploug M, Ronne E, Behrendt N, Jensen AL, Blasi F, Dano K. Cellular receptor for urokinase plasminogen activator. Carboxyl-terminal processing and membrane anchoring by glycosyl-phosphatidylinositol. J Biol Chem 1991;266:1926–33.
5. Moller JV, le Maire M. Detergent binding as a measure of hydrophobic surface area of integral membrane proteins. J Biol Chem 1993;268:18659–72.

6. Cantero D, Friess H, Deflorin J, et al. Enhanced expression of urokinase plasminogen activator and its receptor in pancreatic carcinoma. Br J Cancer 1997;75:388–95.
7. Yamamoto M, Sawaya R, Mohanam S, et al. Expression and localization of urokinase-type plasminogen activator receptor in human gliomas. Cancer Res 1994;54: 5016–20.
8. Gladson CL, Pijuan-Thompson V, Olman MA, Gillespie GY, Yacoub IZ. Up-regulation of urokinase and urokinase receptor genes in malignant astrocytoma. Am J Pathol 1995;146:1150–60.
9. Mohanam S, Sawaya R, McCutcheon I, Ali-Osman F, Boyd D, Rao JS. Modulation of in vitro invasion of human glioblastoma cells by urokinase-type plasminogen activator receptor antibody. Cancer Res 1993;53:4143–7.
10. Reiter LS, Kruithof EK, Cajot JF, Sordat B. The role of the urokinase receptor in extracellular matrix degradation by HT29 human colon carcinoma cells. Int J Cancer 1993;53:444–50.
11. Crowley CW, Cohen RL, Lucas BK, Liu G, Shuman MA, Levinson AD. Prevention of metastasis by inhibition of the urokinase receptor. Proc Natl Acad Sci USA 1993;90:5021–5.
12. Quattrone A, Fibbi G, Anichini E, et al. Antimessenger oligonucleotide for urokinase receptor gene inhibits invasivity of transformed human fibroblasts. Anticancer Drug Des 1995;10:97–102.
13. Mohanam S, Chintala SK, Go Y, et al. In vitro inhibition of human glioblastoma cell line invasiveness by antisense uPA receptor. Oncogene 1997;14:1351–9.
14. Go Y, Chintala SK, Mohanam S, et al. Inhibition of in vivo tumorigenicity and invasiveness of a human glioblastoma cell line transfected with antisense uPAR vectors. Clin Exp Metastasis 1997;15:440–6.
15. Koblinski JE, Ahram M, Sloane BF. Unraveling the role of proteases in cancer. Clin Chim Acta 2000;291:113–35.
16. Watanabe M, Higashi T, Hashimoto M, et al. Elevation of tissue cathepsin B and L activities in gastric cancer. Hepatogastroenterology 1987;34:120–2.
17. Ebert W, Knoch H, Werle B, Trefz G, Muley T, Spiess E. Prognostic value of increased lung tumor tissue cathepsin B. Anticancer Res 1994;14:895–9.
18. Sheahan K, Shuja S, Murnane MJ. Cysteine protease activities and tumor development in human colorectal carcinoma. Cancer Res 1989;49:3809–14.
19. Lah TT, Kokalj-Kunovar M, Strukelj B, et al. Stefins and lysosomal cathepsins B, L and D in human breast carcinoma. Int J Cancer 1992;50:36–44.
20. Rempel SA, Rosenblum ML, Mikkelsen T, et al. Cathepsin B expression and localization in glioma progression and invasion. Cancer Res 1994;54:6027–31.
21. Sinha AA, Wilson MJ, Gleason DF, Reddy PK, Sameni M, Sloane BF. Immunohistochemical localization of cathepsin B in neoplastic human prostate. Prostate 1995; 26:171–8.
22. Guo M, Mathieu PA, Linebaugh B, Sloane BF, Reiners JJ Jr. Phorbol ester activation of a proteolytic cascade capable of activating latent transforming growth factor-ā a process initiated by the exocytosis of cathepsin B. J Biol Chem 2002;277:14829–37.
23. Murphy G, Atkinson S, Ward R, Gavrilovic J, Reynolds JJ. The role of plasminogen activators in the regulation of connective tissue metalloproteinases. Ann NY Acad Sci 1992;667:1–12.
24. Kobayashi H, Ohi H, Sugimura M, Shinohara H, Fujii T, Terao T. Inhibition of in vitro ovarian cancer cell invasion by modulation of urokinase-type plasminogen activator and cathepsin B. Cancer Res 1992;52:3610–4.
25. Montuori N, Mattiello A, Mancini A, et al. Urokinase-mediated posttranscriptional regulation of urokinase-receptor expression in non small cell lung carcinoma. Int J Cancer 2003;105:353–60.
26. Sivaparvathi M, Sawaya R, Wang SW, et al. Overexpression and localization of cathepsin B during the progression of human gliomas. Clin Exp Metastasis 1995;13: 49–56.
27. Mikkelsen T, Yan PS, Ho KL, Sameni M, Sloane BF, Rosenblum ML. Immunolocalization of cathepsin B in human glioma: implications for tumor invasion and angiogenesis. J Neurosurg 1995;83:285–90.
28. Strojnik T, Kos J, Zidanik B, Golouh R, Lah T. Cathepsin B immunohistochemical staining in tumor and endothelial cells is a new prognostic factor for survival in patients with brain tumors. Clin Cancer Res 1999;5:559–67.
29. Demchik LL, Sameni M, Nelson K, Mikkelsen T, Sloane BF. Cathepsin B and glioma invasion. Int J Dev Neurosci 1999;17:483–94.
30. Mohanam S, Jasti SL, Kondraganti SR, et al. Down-regulation of cathepsin B expression impairs the invasive and tumorigenic potential of human glioblastoma cells. Oncogene 2001;20:3665–73.
31. Konduri SD, Yanamandra N, Siddique K, et al. Modulation of cystatin C expression impairs the invasive and tumorigenic potential of human glioblastoma cells. Oncogene 2002;21:8705–12.
32. Mohan PM, Chintala SK, Mohanam S, et al. Adenovirus-mediated delivery of antisense gene to urokinase-type plasminogen activator receptor suppresses glioma invasion and tumor growth. Cancer Res 1999;59:3369–73.
33. Chandrasekar N, Jasti S, Alfred-Yung WK, et al. Modulation of endothelial cell morphogenesis in vitro by MMP-9 during glial-endothelial cell interactions. Clin Exp Metastasis 2000;18:337–42.
34. Weissleder R, Tung CH, Mahmood U, Bogdanov A Jr. In vivo imaging of tumors with protease-activated near-infrared fluorescent probes. Nat Biotechnol 1999;17: 375–8.
35. Mahmood U, Tung CH, Bogdanov A Jr, Weissleder R. Near-infrared optical imaging of protease activity for tumor detection. Radiology 1999;213:866–70.
36. Leunig M, Yuan F, Menger MD, et al. Angiogenesis, microvascular architecture, microhemodynamics, and interstitial fluid pressure during early growth of human adenocarcinoma LS174T in SCID mice. Cancer Res 1992;52:6553–60.
37. Tung CH, Bredow S, Mahmood U, Weissleder R. Preparation of a cathepsin D sensitive near-infrared fluorescence probe for imaging. Bioconjug Chem 1999;10: 892–6.
38. Tung CH, Mahmood U, Bredow S, Weissleder R. In vivo imaging of proteolytic enzyme activity using a novel molecular reporter. Cancer Res 2000;60:4953–8.
39. Hogemann D, Josephson L, Weissleder R, Basilion JP. Improvement of MRI probes to allow efficient detection of gene expression. Bioconjug Chem 2000;11:941–6.
40. Lochter A, Galosy S, Muschler J, Freedman N, Werb Z, Bissell MJ. Matrix metalloproteinase stromelysin-1 triggers a cascade of molecular alterations that leads to stable epithelial-to-mesenchymal conversion and a premalignant phenotype in mammary epithelial cells. J Cell Biol 1997;139:1861–72.
41. Koop S, Khokha R, Schmidt EE, et al. Overexpression of metalloproteinase inhibitor in B16F10 cells does not affect extravasation but reduces tumor growth. Cancer Res 1994;54:4791–7.
42. Van Noorden CJ, Jonges TG, Van Marle J, et al. Heterogeneous suppression of experimentally induced colon cancer metastasis in rat liver lobes by inhibition of extracellular cathepsin B. Clin Exp Metastasis 1998;16:159–67.
43. Hollas W, Soravia E, Mazar A, Henkin J, Blasi F, Boyd D. Decreased urokinase receptor expression by overexpression of the plasminogen activator in a colon cancer cell line. Biochem J 1992;285:629–34.
44. Pedersen H, Brunner N, Francis D, et al. Prognostic impact of urokinase, urokinase receptor, and type 1 plasminogen activator inhibitor in squamous and large cell lung cancer tissue. Cancer Res 1994;54:4671–5.
45. Stahl A, Mueller BM. Binding of urokinase to its receptor promotes migration and invasion of human melanoma cells in vitro. Cancer Res 1994;54:3066–71.
46. Kobayashi H, Schmitt M, Goretzki L, et al. Cathepsin B efficiently activates the soluble and the tumor cell receptor-bound form of the proenzyme urokinase-type plasminogen activator (Pro-uPA). J Biol Chem 1991;266:5147–52.
47. Chapman HA, Wei Y, Simon DI, Waltz DA. Role of urokinase receptor and caveolin in regulation of integrin signaling. Thromb Haemost 1999;82:291–7.
48. Ossowski L, Aguirre-Ghiso JA. Urokinase receptor and integrin partnership: coordination of signaling for cell adhesion, migration and growth. Curr Opin Cell Biol 2000;12:613–20.
49. Yebra M, Goretzki L, Pfeifer M, Mueller BM. Urokinase-type plasminogen activator binding to its receptor stimulates tumor cell migration by enhancing integrin-mediated signal transduction. Exp Cell Res 1999;250:231–40.
50. Wei Y, Yang X, Liu Q, Wilkins JA, Chapman HA. A role for caveolin and the urokinase receptor in integrin-mediated adhesion and signaling. J Cell Biol 1999;144: 1285–94.
51. Graf M, Baici A, Strauli P. Histochemical localization of cathepsin B at the invasion front of the rabbit V2 carcinoma. Lab Invest 1981;45:587–96.
52. Weidner N. Tumour vascularity and proliferation: clear evidence of a close relationship. J Pathol 1999;189:297–9.
53. Keppler D, Sameni M, Moin K, Mikkelsen T, Diglio CA, Sloane BF. Tumor progression and angiogenesis: cathepsin B & Co. Biochem Cell Biol 1996;74:799–810.
54. Kostoulas G, Lang A, Nagase H, Baici A. Stimulation of angiogenesis through cathepsin B inactivation of the tissue inhibitors of matrix metalloproteinases. FEBS Lett 1999;455:286–90.
55. Guo Y, Higazi AA, Arakelian A, et al. A peptide derived from the nonreceptor binding region of urokinase plasminogen activator (uPA) inhibits tumor progression and angiogenesis and induces tumor cell death in vivo. FASEB J 2000;14:1400–10.
56. Li H, Lu H, Griscelli F, et al. Adenovirus-mediated delivery of a uPA/uPAR antagonist suppresses angiogenesis-dependent tumor growth and dissemination in mice. Gene Ther 1998;5:1105–13.